DLL1 orchestrates CD8$^+$ T cells to induce long-term vascular normalization and tumor regression

Naidong Zhang[a,1], Rongping Yin[b,c,d,1], Pei Zhou[a,1], Xiaomei Liu[a,1], Peng Fan[a], Long Qian[a], Li Dong[a,c], Chenglin Zhang[a,c], Xichen Zheng[a], Shengming Deng[a], Jiajie Kuai[a], Zhenhua Liu[a,e], Wen Jiang[f], Xiaohua Wang[c,d,2], Depei Wu[g,2], and Yuhui Huang[a,h,2]

[a]National Clinical Research Center for Hematologic Diseases, Cyrus Tang Medical Institute, Collaborative Innovation Center of Hematology, State Key Laboratory of Radiation Medicine and Prevention, Soochow University, Suzhou 215123, China; [b]College of Medical Technology, Taizhou Polytechnic College, Taizhou 225300, China; [c]Department of Cardiology, the First Affiliated Hospital of Soochow University, Suzhou 215006, China; [d]School of Nursing, Soochow University, Suzhou 215006, China; [e]Department of Radiotherapy, First People's Hospital of Yancheng, Yancheng 224005, China; [f]Department of Radiation Oncology, University of Texas MD Anderson Cancer Center, Houston, TX 77030; [g]National Clinical Research Center for Hematologic Diseases, Jiangsu Institute of Hematology, First Affiliated Hospital of Soochow University, Institute of Blood and Marrow Transplantation of Soochow University, Suzhou 215006, China; and [h]Suzhou Ninth Hospital Affiliated to Soochow University, Suzhou 215200, China

Edited by Guido Kroemer, Institut Gustave Roussy, Villejuif, France, and accepted by Editorial Board Member Tadatsugu Taniguchi April 19, 2021 (received for review October 20, 2020)

The immunosuppressive and hypoxic tumor microenvironment (TME) remains a major obstacle to impede cancer immunotherapy. Here, we showed that elevated levels of Delta-like 1 (DLL1) in the breast and lung TME induced long-term tumor vascular normalization to alleviate tumor hypoxia and promoted the accumulation of interferon γ (IFN-γ)–expressing CD8$^+$ T cells and the polarization of M1-like macrophages. Moreover, increased DLL1 levels in the TME sensitized anti-cytotoxic T lymphocyte–associated protein 4 (anti-CTLA4) treatment in its resistant tumors, resulting in tumor regression and prolonged survival. Mechanically, in vivo depletion of CD8$^+$ T cells or host IFN-γ deficiency reversed tumor growth inhibition and abrogated DLL1-induced tumor vascular normalization without affecting DLL1-mediated macrophage polarization. Together, these results demonstrate that elevated DLL1 levels in the TME promote durable tumor vascular normalization in a CD8$^+$ T cell– and IFN-γ–dependent manner and potentiate anti-CTLA4 therapy. Our findings unveil DLL1 as a potential target to persistently normalize the TME to facilitate cancer immunotherapy.

Delta-like 1 | long-term tumor vascular normalization | tumor microenvironment | cancer immunotherapy

One of the major challenges currently facing cancer treatments is the aberrant tumor microenvironment (TME), characterized as hypoxia, immunosuppression, acidity, and high interstitial fluid pressure (IFP) (1–5). These properties render tumors resistant to many kinds of cancer treatment modalities. High IFP prevents the penetration and distribution of drug agents into the tumor parenchyma, while hypoxia compromises the effectiveness of chemotherapy and radiotherapy because both treatment modalities often require reactive oxygen species to evoke antitumor activities (4, 6). In addition, hypoxia induces the secretion of multiple immune inhibitory factors and promotes the accumulation of immune regulatory cell populations, such as transforming growth factor-β (TGF-β), interleukin 10 (IL10), myeloid-derived suppressor cells (MDSCs), M2-like tumor-associated macrophages (M2-TAMs), and regulatory T cells (Tregs) (1, 3, 7–9). Thus, the hypoxic and immunosuppressive TME hinders cancer immunotherapy to efficiently eradicate cancer cells.

Emerging evidence suggests that the abnormal tumor vasculature contributes largely to the aberrant TME (1, 3, 4). Tumor blood vessels are tortuous, dilated, and leaky with low pericyte coverage. The resulting blood flow is often static and fluctuated and therefore creates a hypoxic and acidic TME with high IFP (4). Therefore, tumor vascular normalization has been proposed as a promising approach to alleviate the aberrances within the TME, thus enhancing the efficacy of a range of cancer treatment modalities, including chemotherapy, radiotherapy, and immunotherapy (10–18). Vascular endothelial growth factor (VEGF) ligands and receptors constitute one of the most potent proangiogenic signaling pathways (19). Various VEGF signaling inhibitors, such as Bevacizumab and Cediranib, have been approved to treat several types of cancers. VEGF signaling inhibitors can induce tumor vascular normalization; however, the duration of the normalization is usually transient, and therefore, the improvement to the concurrent chemotherapy and immunotherapy is marginal (4, 19–21). In addition, many kinds of cancer are intrinsically resistant to VEGF signaling targeted therapy (4, 19). Thus, novel approaches are needed to induce tumor vascular normalization for longer periods and in broad tumor types.

The evolutionarily conserved Notch signaling pathway plays critical roles in cell differentiation and blood vessel formation. The Notch signaling pathway consists of four Notch receptors (Notch 1 to 4) and four ligands (Jagged1, Jagged2, Delta-like 1 [DLL1], and DLL4) in murine (22). Both Notch receptors and ligands are membrane proteins. DLL1, DLL4, and Jagged1 have been shown to express in endothelial cells and play important roles in vascular development and postnatal vessel formation (23, 24). DLL1 and

Significance

Cancer immunotherapy demonstrates durable clinical efficacy but only in a small percentage of cancer patients. The aberrant tumor blood vessels and resulting hypoxic tumor microenvironment are major obstacles to hinder cancer immunotherapy. Tumor vascular normalization is a promising strategy to overcome these hindrances; however, the normalizing effects induced by current available approaches are often transient, limiting its therapeutic benefits. Here, we show that Delta-like 1 (DLL1) can induce long-term tumor vascular normalization, alleviate the hypoxia and immunosuppression within the tumor microenvironment, and prolong survival of anti-CTLA4 therapy. This study suggests that DLL1 is a potential target to persistently normalize the tumor microenvironment to enhance cancer immunotherapy.

Author contributions: X.W., D.W., and Y.H. designed research; N.Z., R.Y., P.Z., X.L., P.F., L.Q., L.D., C.Z., X.Z., S.D., J.K., Z.L., and Y.H. performed research; N.Z., R.Y., P.Z., X.L., P.F., L.Q., Z.L., W.J., and Y.H. analyzed data; and W.J., X.W., D.W., and Y.H. wrote the paper.

The authors declare no competing interest.

This article is a PNAS Direct Submission. G.K. is a guest editor invited by the Editorial Board.

[1]N.Z., R.Y., P.Z., and X.L. contributed equally to this work.

[2]To whom correspondence may be addressed. Email: huangyh@suda.edu.cn, wudepei@suda.edu.cn, or sxwang2001@163.com.

This article contains supporting information online at https://www.pnas.org/lookup/suppl/doi:10.1073/pnas.2020057118/-/DCSupplemental.

Published May 25, 2021.

DLL4 are also associated with tumor angiogenesis (24–26). DLL4 is usually expressed in tumor endothelial cells but rarely in tumor cells (27, 28). Blockade of DLL4 suppresses tumor growth through the induction of nonfunctional tumor vessel formation (24, 25, 29). Thus, activation of DLL4/Notch signaling has the potential to increase tumor vascular maturation. Indeed, higher expression of DLL4 in bladder tumor endothelial cells was correlated with vessel maturation (30). Unfortunately, long-term DLL4 blockade led to vascular neoplasms, and persistent activation of DLL4/Notch signaling promoted T cell acute lymphoblastic leukemia (T-ALL) (31–33).

Because of these potential safety concerns of chronic blockade or activation of DLL4/Notch signaling, we proposed instead to remodel tumor vessels via the activation of DLL1/Notch signaling. In contrast to the extensive attention of DLL4 in tumor angiogenesis, the roles of DLL1 in tumor vessel formation is largely unknown. Here, we showed that overexpression of DLL1 in EO771 breast and LAP0297 lung tumor cells not only induced durable tumor vascular normalization but also stimulated $CD8^+$ T cell activities. Interestingly, in vivo depletion of $CD8^+$ T cells prior to tumor implantation or host IFN-γ deficiency abrogated the effects of DLL1 overexpression on tumor vessels, suggesting that selective activation of DLL1/Notch signaling induces long-term tumor vascular normalization via T cell activation. Moreover, DLL1/Notch signaling activation in combination with anti-CTLA4 therapy prolonged survival. Thus, this study uncovered DLL1 as a potential target to induce long-term tumor vascular normalization to enhance cancer immunotherapy.

Results

Elevated Levels of DLL1 in the TME Induce Long-Term Tumor Vascular Normalization. Tumor vascular normalization is a promising strategy to potentiate concurrent antitumor treatments; however, the short duration of the normalizing effects limits its benefits (4, 12, 18). Previous studies showed that systemic blockade of DLL4 promoted nonfunctional tumor vessel formation (25, 29). Thus, we hypothesized that DLL1 elevation in the TME induces tumor vascular normalization. To increase DLL1 levels in the TME, we cloned the murine DLL1 gene into a lentivirus expression system carrying green fluorescent protein (GFP) and established DLL1-overexpressing and mock-transfected EO771 breast tumor cell lines, named as EO771-L1 and EO771-R1, respectively (*SI Appendix*, Fig. S1*A*). Both Western blotting and qPCR data showed that the levels of DLL1 were increased in EO771-L1 tumor cells compared to EO771-R1 tumor cells (*SI Appendix*, Fig. S1 *B* and *C*). In addition, *Hes1*, a Notch signaling downstream gene, was significantly up-regulated in EO771-L1 tumor tissues as compared to EO771-R1 tumor tissues (*SI Appendix*, Fig. S1*C*), indicating that overexpression of DLL1 in tumor cells activated Notch signaling in the TME. In vitro, DLL1 overexpression slightly suppressed tumor cell proliferation without affecting apoptosis (*SI Appendix*, Fig. S2). In vivo, DLL1 overexpression significantly inhibited EO771-L1 tumor growth compared to EO771-R1 control tumors (Fig. 1*A*). DLL1 overexpression was also found to decrease vessel density and tortuosity, while pericyte coverage and global vessel perfusion were increased, accompanied with significantly reduced tissue hypoxia and vessel leakage in EO771-L1 tumors compared to EO771-R1 tumors, demonstrating tumor vascular normalization (Fig. 1 *B* and *C* and *SI Appendix*, Figs. S3 and S4).

To test the duration of vascular normalization as well as the distribution of functional tumor blood vessels upon DLL1 overexpression, we performed tumor size matched experiments by harvesting EO771-R1 and EO771-L1 tumors when their size reached 4 to 5, 6 to 7, and 8 to 9 mm in diameter, respectively. Vascular function analyses showed that the overall tumor vessel perfusion in cross-sections of tumor tissues was significantly higher in EO771-L1 tumors compared with EO771-R1 tumors from all three tumor size groups (Fig. 2). In EO771-R1 tumors, functional blood vessels (Ho 33342 positive) were generally clustered in the tumor margin, especially in larger tumors. In contrast, functional blood vessels were more evenly distributed across entire tumor parenchyma in EO771-L1 tumors, even in the 8 to 9 mm group, corresponding to a 3-wk post–tumor cell inoculation (Fig. 2*A*). The overall tumor vessel perfusion decreased rapidly as tumor sizes increased in EO771-R1 tumors but remained persistently elevated in EO771-L1 tumors (Fig. 2*B*). Together, these data demonstrate that elevated levels of DLL1 in the TME induces durable tumor vascular normalization.

DLL1 Elevation in the TME Reduces Immunosuppressive Immune Cell Populations and Activates $CD8^+$ T Cells. Our previous work showed that overexpression of DLL1 in hematopoietic progenitor cells stimulated Notch signaling in the hematopoietic microenvironments and enhanced T cell immunity (34). To understand the influences of DLL1 elevation on the tumor immune microenvironment, we analyzed tumor-infiltrating immune cell populations. Myeloid cell populations are often the major immune components in the TME in breast tumors. DLL1 elevation in the TME increased the proportions of TAMs in EO771 tumors (*SI Appendix*, Fig. S5). TAM is highly plastic with a continuum of phenotypes, of which M1- and M2-like TAMs represent two extreme phenotypes. CD11c and CD206 (also MRC1) are commonly used markers for the identification of M1- and M2-like TAMs, respectively (35, 36). Remarkably, elevated levels of DLL1 in the TME dramatically polarized TAMs toward an M1-like phenotype (EO771-R1: 24.93% M1-TAMs and 22.04% M2-TAMs in total TAMs; EO771-L1: 60.96% M1-TAMs and 1.39% M2-TAMs in total TAMs) (*SI Appendix*, Fig. S5). Moreover, DLL1 overexpression slightly reduced the proportions of Treg ($CD4^+CD25^+Foxp3^+$) and $CD4^+CD279^+$ T cells, though it did not change the proportion of tumor-infiltrating $CD4^+$ T cells (Fig. 3*A* and *SI Appendix*, Fig. S6). These results suggest that DLL1 overexpression in the TME decreases immunosuppressive immune cell populations. In line with the alleviation of immunosuppression, DLL1 overexpression increased tumor-infiltrating $CD8^+$ T cells and effector memory $CD8^+$ T cells ($CD8^+CD44^+CD62L^-$) without affecting central memory $CD8^+$ T cells ($CD8^+CD44^+CD62L^+$) (Fig. 3 *A*–*E*). In addition, DLL1 overexpression increased IFN-γ production in $CD8^+$ T cells but not $CD4^+$ T cells (Fig. 3 *D* and *G*). qPCR data further showed that the transcription of genes related to antitumor immune responses, such as *Ifng*, *Cxcl9*, *Tnfa*, *Gzmb*, and *Prf1*, were up-regulated in EO771-L1 tumors compared to control EO771-R1 tumors (*SI Appendix*, Fig. S7). Meanwhile, activated Notch 1 was observed in $F4/80^+$, $CD4^+$, $CD8^+$, and $CD31^+$ cells in EO771-L1 tumors but rarely in EO771-R1 tumors and neither in GFP^+ tumor cells (*SI Appendix*, Figs. S8 and S9). The transcription of Notch signaling target genes *Hes5* and *Deltex1* was up-regulated in $CD8^+$ T cells and TAMs isolated from EO771-L1 tumors compared to EO771-R1 tumors (*SI Appendix*, Fig. S10), indicating the activation of Notch signaling in $CD8^+$ T cells and TAMs upon DLL1 overexpression. Together, these data show that elevated levels of DLL1 in the TME promote the accumulation and activation of $CD8^+$ T cells within the tumor parenchyma.

DLL1 Overexpression Normalizes Tumor Blood Vessels and Promotes $CD8^+$ T Cell Accumulation in Lung Carcinoma. To test whether increased DLL1 levels in the TME will have similar effects in other tumor types, we transfected LAP0297 lung carcinoma cells and established DLL1 overexpressing LAP0297 cells (LAP-L1) or mock control LAP0297 cells (LAP-R1). Consistent with the breast tumor model, DLL1 overexpression in LAP0297 carcinoma cells suppressed tumor growth and promoted the accumulation of tumor-infiltrating $CD8^+$ T cells compared to LAP-R1 (Fig. 4 *A* and *B*). Elevated levels of DLL1 in lung carcinoma TME also reduced tumor vessel density, increased global vessel perfusion, decreased tissue hypoxia, and induced long-term tumor vascular normalization (Fig. 4*C* and *SI Appendix*, Figs. S11 and S12). These data suggest

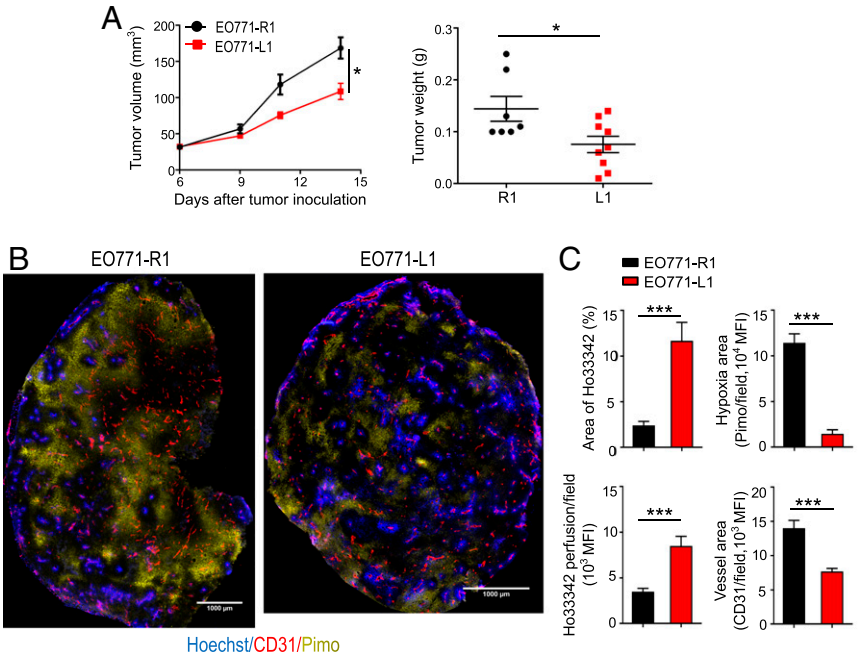

Fig. 1. Elevated levels of DLL1 in the TME inhibits EO771 breast tumor growth and induces tumor vascular normalization. EO771 murine breast tumor cells overexpressing DLL1 (EO771-L1 or L1) or mock control (EO771-R1 or R1) (2×10^5 cells) were orthotopically inoculated into the mammary fat pad of female C57BL/6 mice. Tumor size was measured every 3 d. The tumor volume was estimated by the formula [(long axis) × (short axis)^2 × π/6]. Mice were intravenously injected with 1.2 mg/mouse pimonidazole (Pimo) 25 min and 200 μg/mouse Hoechst 33342 (Ho33342) 5 min before tumor harvest. (*A*) The tumor growth curves and tumor weight of EO771-R1 and EO771-L1. (*B*) Representative figures showing Pimo staining and Ho33342 perfusion. (*C*) The statistical analysis of tumor vessel perfusion (Ho33342), tumor hypoxia (Pimo), and vessel density (CD31) in EO771-R1 and EO771-L1 breast tumors. (Scale bars, 1,000 μm.) Ho33342 (blue), Hoechst 33342 perfused tumor area; CD31 (red), endothelial cells; Pimo (yellow), hypoxic tumor area; MFI, mean fluorescence intensity. Significance was determined by unpaired two-tailed Student's *t* tests. Data are from one experiment representative of three (in *A*, $n = 7$ to 9 mice per group) or two (in *B* and *C*, $n = 8$ to 10 mice per group) independent experiments with similar results. All data are presented as means ± SEM, $*P < 0.05$, $***P < 0.001$.

that the tumor vascular normalizing effect of DLL1 augmentation is applicable to different tumor types.

CD8$^+$ T Cells Mediate the Effects of DLL1 Elevation on Tumor Blood Vessels via IFN-γ. Our recent studies as well as others showed that activated T cells by immune checkpoint blockade (ICB) were able to induce tumor vascular normalization (37, 38). As DLL1 overexpression activated CD8$^+$ T cells, we next investigated whether T cells mediate vessel remodeling by the elevated levels of DLL1 in the TME. In vivo depletion of CD4$^+$ and CD8$^+$ T cells simultaneously or CD8$^+$ T cells alone did not affect tumor growth in EO771-R1 tumors yet completely reversed the tumor growth inhibition in EO771-L1 tumors (Fig. 5*A* and *SI Appendix*, Figs. S13 and S14*A*). Meanwhile, in vivo depletion of CD4$^+$ and CD8$^+$ T cells simultaneously reversed the effects of DLL1 overexpression on tumor vessel density and tumor vessel perfusion (Fig. 5 *B* and *C*). Interestingly, in vivo depletion of CD8$^+$ T cells alone reversed the effects of DLL1 overexpression on tumor vessel perfusion but not tumor vessel density (*SI Appendix*, Fig. S14 *B* and *C*). This could be due to the impact of DLL1 on CD8$^+$ T cells during tumor initiation. We then performed CD8$^+$ T cell depletion prior to EO771 tumor cell inoculation. Indeed, CD8$^+$ T cell depletion before tumor engraftment completely negated the effects of DLL1 overexpression on tumor vessel density and tumor vessel perfusion (*SI Appendix*, Fig. S15) but did not reverse M1-TAM polarization by DLL1 overexpression (*SI Appendix*, Fig. S16*A*). Next, we asked whether IFN-γ is the effective molecule of CD8$^+$ T cells during this pathological process. We then implanted EO771-R1 and EO771-L1 tumor cells in both wild-type (WT) and IFN-γ$^{-/-}$ mice. Murine IFN-γ deficiency did not alter tumor growth and vascular characteristics in EO771-R1 tumors but abolished the impacts of DLL1 overexpression on tumor growth, tumor vessel density, and tumor vessel perfusion in EO771-L1 tumors (Fig. 6). Again, DLL1 overexpression exhibited comparable ability to polarize TAM from an M2- to M1-like phenotype in both WT and IFN-γ$^{-/-}$ mice (*SI Appendix*, Fig. S16*B*). Together, these data demonstrate that elevated DLL1 levels in the TME induce tumor vascular normalization via the activation of CD8$^+$ T cells and the production of IFN-γ.

Elevated Levels of DLL1 in the TME Sensitize Tumors to Anti-CTLA4 Therapy. Cancer immunotherapy has demonstrated its durable therapeutic efficacy but only in a small percent of cancer patients (39, 40). The hypoxic and immunosuppressive TME is a key obstacle that hinders cancer immunotherapy (1–4). As elevated DLL1 levels normalize tumor vessels and reduce immunosuppression in the TME, we reasoned that DLL1 enhances anti-CTLA4 therapy. Remarkably, anti-CTLA4 therapy induced EO771-L1 tumor regression and significantly prolonged survival compared to EO771-L1 with control IgG treatments, while anti-CTLA4 therapy did not affect much on EO771-R1 tumor growth (Fig. 7 *A* and *B*). Treg reduction is one of the mechanisms mediated by the therapeutic effects of anti-CTLA4 treatments in solid tumors (41, 42). Our data show that about 80% of CD4$^+$ T cells are Tregs in EO771 tumors (*SI Appendix*, Fig. S6*C*). Indeed, in vivo depletion of CD4$^+$ T cells rapidly induced EO771-L1 tumor regression and significantly prolonged survival compared to EO771-R1 tumors (Fig. 7 *C* and *D*). Together, these data suggest that elevated DLL1 levels improve anti-CTLA4 therapy. Currently, the combination of ICB therapy and antiangiogenic treatments exhibits encouraging clinical benefits (21, 43). Since DLL1 can persistently normalize tumor blood vessels and create an immune stimulatory microenvironment, selective activation of DLL1/Notch signaling may provide a novel strategy to potentiate ICB therapy.

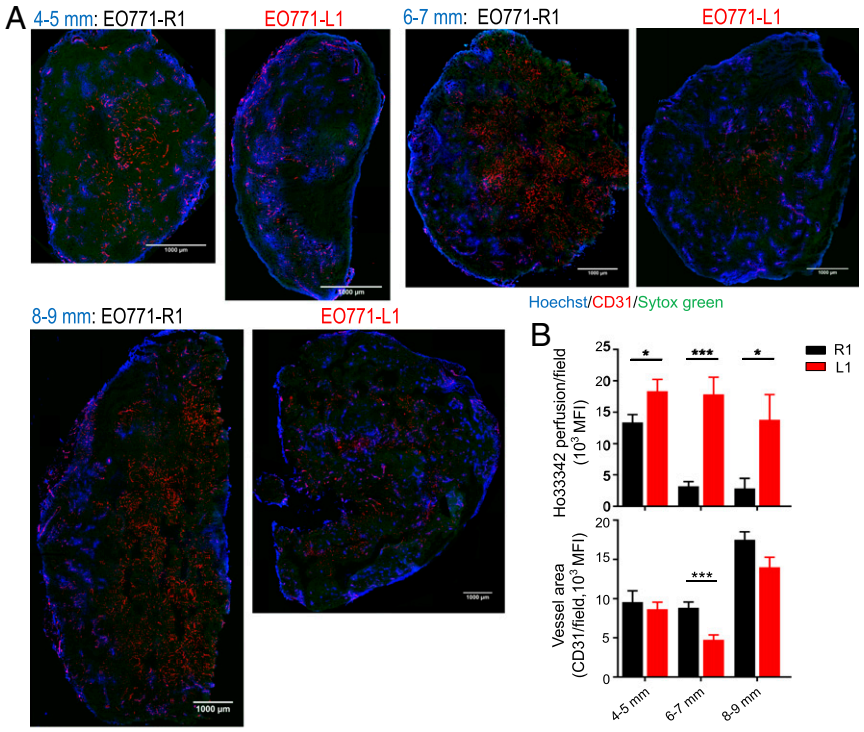

Fig. 2. DLL1 elevation in the TME induces long-term tumor vascular normalization. EO771-R1 and EO771-L1 breast tumors were prepared as described in Fig. 1. Tumor tissues were harvested when their sizes reached 4 to 5, 6 to 7, and 8 to 9 mm in diameter, respectively. Vessel perfusion over the entire cross-section of tumor tissues was assessed by confocal microscopy. (*A*) Representative whole tumor tissue perfusion images. (Scale bars, 1,000 μm.) (*B*) Vessel perfusion and vessel density in indicated sizes of EO771-R1 and EO771-L1 tumors. Ho33342 (blue), Hoechst 33342 perfused area; CD31 (red), endothelial cells; and Sytox Green (green), counterstained for tumor tissue. Significance was determined by unpaired two-tailed Student's *t* tests. Each group had 8 to 10 mice. $*P < 0.05$, $***P < 0.001$.

Discussion

The aberrant tumor vasculature not only impedes the deliver and distribution of antitumor agents into tumor parenchyma but also creates a hypoxic TME which compromises the effectiveness of cancer treatments. Thus, to improve tumor vascular function could overcome these abnormalities and enhance the effectiveness of concurrent antitumor treatments (10, 11, 15, 44). However, the duration of tumor vascular normalization is usually transient (45, 46). In this study, we found that increased levels of DLL1 in the TME induced durable tumor vascular normalization and polarized the tumor immune microenvironment away from immunosuppression toward an immune stimulatory status, resulting in the activation of $CD8^+$ T cells. In vivo depletion of $CD8^+$ T cells or host IFN-γ deficiency abrogated vascular remodeling by DLL1 overexpression. Moreover, DLL1 overexpression sensitized anti-CTLA4 therapy. Our study uncovered a potential strategy to persistently normalize tumor blood vessels and the TME. Therefore, selective activation of DLL1/Notch signaling within the TME might represent a new approach to elicit long-term vascular normalization to potentiate concurrent cancer treatments.

Currently available approaches usually induce transient vascular normalization with the duration of around 2 to 8 d in preclinic tumor models, limiting their beneficial effects on anticancer treatments, especially cancer immunotherapy (45, 46) because cancer immunotherapy usually needs more than 1 wk to activate antitumor immune responses and a longer time to achieve therapeutic efficacy. The short duration of vascular normalization upon antiangiogenic therapy could be due to its standard high dose regime or the influences of complementary proangiogenic factors (45, 46). By increasing DLL1 levels in the TME, we observed normalized tumor blood vessels from small (4 to 5 mm) to big (7 to 8 mm) EO771 breast tumors with the duration of more than 3 wk. The effects of DLL1 on tumor blood vessels is mediated by $CD8^+$ T cells via IFN-γ. IFN-γ seems to have long-lasting anti-angiogenic effects and cannot be reversed by other proangiogenic factors (47). This could be a reason that DLL1 could induce durable tumor vascular normalization.

Hypoxia is a hallmark of TME. The immunosuppressive characteristics of hypoxia were derived from the facts that hypoxia suppresses $CD8^+$ T cell differentiation and that hypoxia elevates adenosine in the TME, which exerts immunosuppression via adenosine receptors (A2AR and A2BR) (6, 48–51). Thus, eliminating hypoxia/adenosine through respiratory hyperoxia, vascular normalization, or antagonists to A2AR and HIF-1α potentiates cancer immunotherapy (Fig. 7) (5, 6, 8, 52). However, hypoxia elimination by HIF-1α inhibitor PX478 (53) treatments neither further reduced tissue hypoxia nor enhanced the antitumor effects of DLL1 overexpression in EO771 tumors (*SI Appendix*, Fig. S17), suggesting that the combination of different anti-hypoxia approaches simultaneously might not yield additive hypoxia elimination to achieve better antitumor effects. Meanwhile, we need to be aware that HIF-1α is controlled not only by environmental oxygen but also by infection and inflammatory cytokines. Therefore, the impacts of a hypoxic environment and HIF-1α itself could be different in different types of cells via different mechanisms. HIF-1α within $CD8^+$ T cells have been shown to enhance glycolysis and induce the expression of cytotoxicity-related factors, including IFN-γ, granzyme B, and TNF-α, thus suppressing tumor growth (54, 55). In some nontumoral inflammatory condition, like wounds and abscesses, HIF-1α is essential for myeloid cell-mediated inflammation through regulating their glycolytic energy production (56). Thus, distinct strategies are necessary to better cope with hypoxia for promoting host immunity against different diseases.

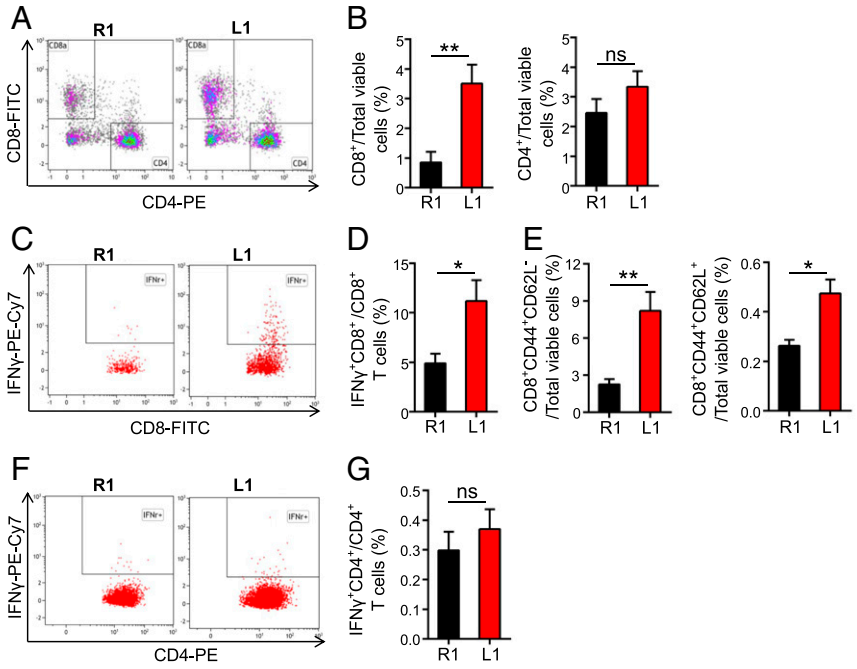

Fig. 3. Elevated DLL1 levels in the TME promote the accumulation and activation of $CD8^+$ T cells in EO771 breast tumors. EO771-R1 and EO771-L1 breast tumors were prepared as described in Fig. 1. Tumor-infiltrating immune cells were analyzed by flow cytometry. The doublet/aggregated events were gated out using side scatter area versus side scatter width. Dead cells were excluded by 7-AAD staining. Lymphoid cells in $CD45^+CD11b^-$ cells were analyzed with expression of CD8 and CD4. (*A* and *B*) The proportions of tumor-infiltrating $CD8^+$ and $CD4^+$ T cells. (*C* and *D*) IFN-γ production in tumor-infiltrating $CD8^+$ T cells. (*E*) The proportions of effector memory ($CD8^+CD44^+CD62L^-$) and central memory ($CD8^+CD44^+CD62L^+$) $CD8^+$ T cells in EO771-R1 and EO771-L1 breast tumors. (*F* and *G*) IFN-γ production in tumor-infiltrating $CD4^+$ T cells. The significance was determined by unpaired two-tailed Student's *t* tests. Data are from one experiment representative of three independent experiments with similar results ($n = 7$ to 9 mice per group). All data are presented as means ± SEM, $^*P < 0.05$, $^{**}P < 0.01$, ns, no significant difference.

Previous reports suggested that DLL1/Notch activation was antiangiogenic based on a reduction in tumor vessel density (57, 58). Vessel density is one common parameter to evaluate the effects of an agent on the tumor vasculature. Decreased vessel density can happen in either vessel pruning or vascular normalization. Thus, other vascular parameters are important to get more insight into the impact of an intervention on tumor blood vessels. For example, vessel perfusion, hypoxia, and pericyte coverage are critical to evaluate the integrity and function of tumor vessels. Whether an intervention could improve tumor vessel function is a major parameter to distinguish vessel pruning and vascular normalization (11, 15, 45, 46). In our tumor models, we found that elevated DLL1 levels in the TME enhanced tumor vessel perfusion beside vessel density reduction, indicating vascular normalization. Moreover, we demonstrated that DLL1/Notch activation induced tumor vascular normalization via T cell stimulation. These results indicate that the primary effects of DLL1 elevation in the TME are immune cell modulation. This is consistent with a recent study showing that multivalent clustered DLL1-triggered Notch signaling elicits antitumor immunity in lung cancer (59). Under tumor condition, DLL4, but not DLL1, is often up-regulated in tumor endothelial cells. Blockade of DLL4 had impacts on both tumor vessels and T cells, but it is unclear whether T cells mediate the effects of DLL4 blockade on tumor angiogenesis.

Our previous study showed that tumor growth inhibited expression of DLL1 and DLL4 in the hematopoietic environments, which mediated tumor-associated T cell immunosuppression (34). Overexpressing DLL1 in bone marrow progenitor cells suppressed tumor growth in a $CD8^+$ T cell–dependent manner (34). In this study, we showed that the overexpression of DLL1 in tumor cells also suppressed tumor growth, and the depletion of $CD8^+$ T cells abrogated such tumor growth inhibition. In line with this result, the overexpression of DLL1 in tumor cells increased the presence of $CD8^+$ T cells within the TME and elevated IFN-γ production. Whether DLL1 could directly induce IFN-γ expression in $CD8^+$ T cells is unknown. As DLL1 overexpression reduced immunosuppressive immune cell populations, including M2-TAMs, Tregs, and PD1-positive $CD4^+$ T cells, it is possible that decreased immunosuppression and hypoxia within the TME resuscitated $CD8^+$ T cell activities.

The Delta family ligands signaling through Notch receptors exert critical roles in neonatal and postnatal vessel formation. Elevated DLL1 levels in the TME stimulated $CD8^+$ T cell activities and induced long-term tumor vascular normalization and therefore retarded tumor growth. Moreover, the remodeling of DLL1 overexpression in the TME converted nonresponsive tumors to become sensitive to anti-CTLA4 therapy. This study indicated a strategy to durably normalize tumor blood vessels and to potentiate the efficacy of immune checkpoint therapy.

Materials and Methods

Mice and Tumor Treatments. Female C57BL/6 mice (6 to 8 wk old) were purchased from Beijing Vital River Laboratory Animal Technology Co., Ltd. (the joint venture of Charles River Laboratories in China). IFN-$\gamma^{-/-}$ C57BL/6 mice were purchased from Jackson Laboratories. Foxp3-eGFP C57BL/6 mice were a generous gift from Zhinan Yin, Jinan University, Guangzhou, China. FVB mice (an inbred mouse strain named for its susceptibility to Friend leukemia virus B) were bred in the specific pathogen-free (SPF) animal facility at Soochow University. EO771 breast tumor cells overexpressing DLL1 (EO771-L1) or mock control (EO771-R1) (2×10^5 cells) were orthotopically inoculated into the third mammary fat pad of C57BL/6 mice. LAP0297 lung cancer cells overexpressing DLL1 (LAP-L1) or mock control (LAP-R1) (2×10^5 cells) were inoculated subcutaneously into the right flank of female FVB mice. The tumor size was measured every 3 d using a caliper, and the tumor volume was estimated by the formula [(long axis) × (short axis)^2 × π/6].

In vivo T cell depletion was performed according to our previous publication (37). Briefly, mice were injected intraperitoneally with 200 μg anti-CD8a monoclonal antibody (53-6.72, Bio X Cell) and anti-CD4 monoclonal

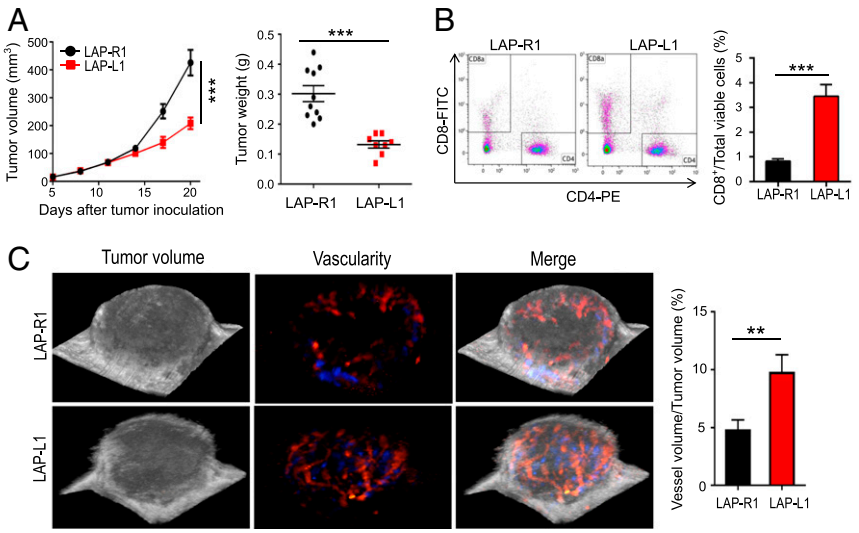

Fig. 4. Increased levels of DLL1 in the TME inhibits LAP0297 lung tumor growth and induces tumor vascular normalization. LAP0297 murine lung cancer cells overexpressing DLL1 (LAP-L1) or mock control (LAP-R1) (2×10^5 cells) were inoculated subcutaneously in the right flank of female FVB mice. Tumor size was recorded and analyzed as described in Fig. 1. Murine ultrasonographic imaging was conducted to measure global tumor vessel perfusion by using a 3D imaging motor and color Doppler mode. (*A*) The tumor growth curves and tumor weight of LAP-R1 and LAP-L1. (*B*) The proportions of tumor-infiltrating $CD8^+$ and $CD4^+$ T cells were analyzed by flow cytometry. (*C*) The percentages of global tumor blood volume in 3D tumor volume were analyzed. The blue and red colors represent different blood flow directions. The significance was determined by unpaired two-tailed Student's *t* tests. Data are from one experiment representative of three independent experiments with similar results ($n = 8$ to 10 mice per group). All data are presented as means ± SEM, $^{**}P < 0.01$, $^{***}P < 0.001$.

antibody (GK1.5, Bio X Cell) or 200 μg isotype-matched control antibody IgG2a (2A3, Bio X Cell) on days 6, 8, and 14 after tumor cell inoculation. In some experiments, anti-CD8a monoclonal antibody was injected on days −1, 1, 7, and 13 upon tumor cell inoculation. The efficiency of T cell depletion was assessed by flow cytometry at the end of the experiment.

All animal studies were approved by the Institutional Laboratory Animal Care and Use Committee of Soochow University. Mice were kept in a SPF facility in individual ventilated cages. All experimental methods were conducted in accordance with the Animal Care and Use Regulations of China.

Tumor Cell Culture. The EO771 murine breast tumor and human embryonic kidney (HEK) 293T cell lines were ordered from the CH3 Biosystems and the American Type Culture Collection, respectively. The LAP0297 lung carcinoma cell line was generated by Peigen Huang at Massachusetts General Hospital

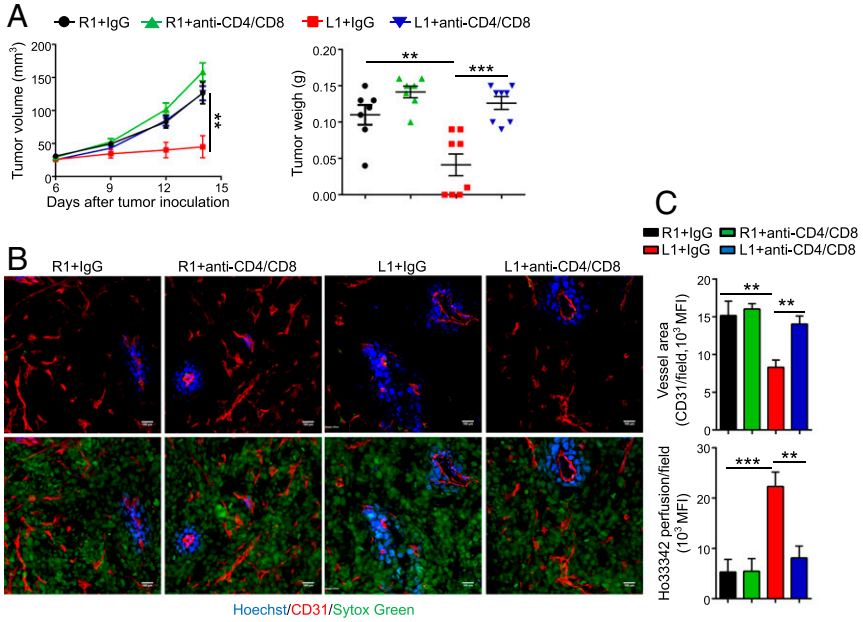

Fig. 5. In vivo depletion of T cells reverses the improvement of vessel perfusion and the inhibition of tumor growth induced by DLL1 overexpression in EO771 breast tumor model. EO771-R1 and EO771-L1 breast tumors were prepared as described in Fig. 1. Mice were randomly assigned to two groups and treated with anti-CD8 and anti-CD4 antibodies or control IgG (200 μg/mouse) on days 6 (the corresponding tumor sizes were 3 to 4 mm in diameter), 8, and 14 post–tumor cell inoculation, respectively. (*A*) The tumor growth curves and tumor weight. (*B* and *C*) Tumor blood vessel perfusion and vessel density in EO771-R1 and EO771-L1 breast tumors without or with T cell depletion. (Scale bars, 100 μm.) The significance was determined by one-way ANOVA. Data are from one experiment representative of two independent experiments with similar results ($n = 7$ to 8 mice per group). $^{**}P < 0.01$, $^{***}P < 0.001$.

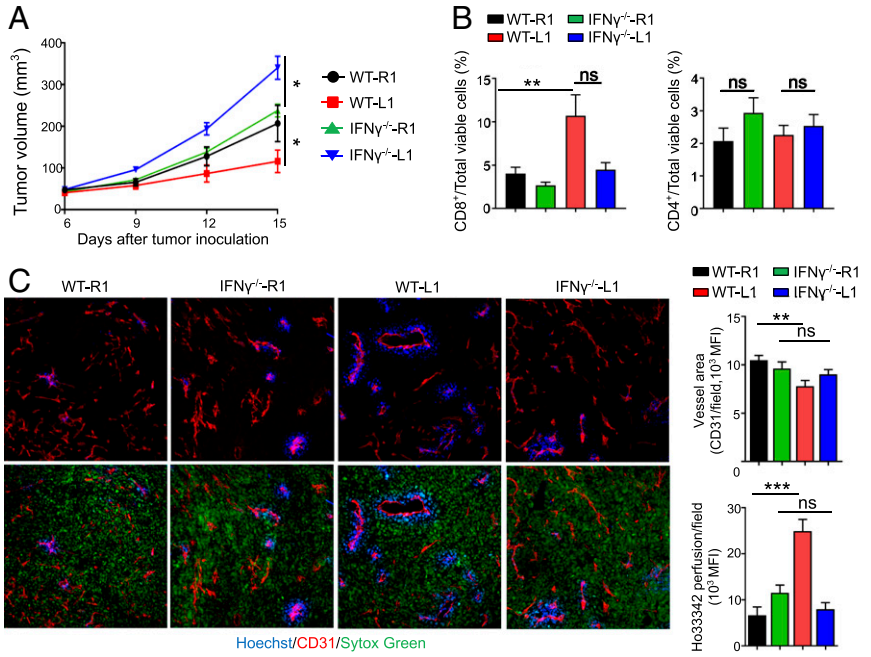

Fig. 6. IFN-γ deficiency negates the effects of DLL1 overexpression on tumor growth, CD8$^+$ T cell tumor infiltration, and vessel perfusion in EO771 breast tumor model. EO771-R1 and EO771-L1 breast tumor cells were inoculated orthotopically in WT and IFN-γ knockout mice (IFN-γ$^{-/-}$). Tumor size and tumor blood vessel perfusion were recorded and analyzed as described in Fig. 1. (*A*) The tumor growth curves. (*B*) The proportions of tumor-infiltrating CD8$^+$ and CD4$^+$ T cells. (*C*) Tumor blood vessel perfusion and vessel density in EO771-R1 and EO771-L1 breast tumors in WT or IFN-γ$^{-/-}$ mice. The significance was determined by one-way ANOVA. Data are from one experiment representative of three independent experiments with similar results (n = 7 to 8 mice per group). *$P < 0.05$, **$P < 0.01$, ***$P < 0.001$, ns, no significant difference.

(60). All the cell lines were maintained in Dulbecco's Modified Eagle Medium (DMEM; Gibco) containing 10% fetal bovine serum (Gibco) and 1% Penicillin-Streptomycin (Gibco). Cell cultures were frequently monitored for mycoplasma contamination, and only mycoplasma-negative cells were used for experiments.

***Dll1* Overexpression.** The murine *Dll1* gene was cloned into the retrovirus plasmid MigR1 carrying GFP. The successful insertion of the *Dll1* gene in the new MigR1-DLL1 plasmid was confirmed by restriction enzyme digestion and DNA sequencing. The retrovirus particles were generated by transfecting HEK 293T cells with plasmids (MigR1 and MigR1-DLL1) using calcium chloride (Sigma). EO771 and LAP0297 tumor cell lines were infected with retrovirus particles. Stably infected cell lines (EO771-R1, EO771-L1, LAP-R1, and LAP-L1) were obtained by flow sorting (FACS Aira III flow cytometer, BD Bioscience). DLL1 overexpression was determined by Western blotting.

Western Blot. The fractions of membrane or cytosol protein were extracted from EO771-R1 and EO771-L1 cell lines by using a Membrane and Cytosol Protein Extraction Kit (Beyotime) according to the manufacturer's instructions. The protein concentrations were determined using the BCA Protein Assay reagents (Beyotime). The protein was then separated by sodium dodecyl sulfate–polyacrylamide gel electrophoresis and transferred onto a polyvinylidene difluoride membrane. The membrane was blocked with 5% skimmed milk and then incubated with a primary rabbit polyclonal antibody against DLL1 (Delta [H265]: sc-9102) followed with horseradish peroxidase (HRP) conjugated secondary antibodies (goat anti-rabbit HRP, Multisciences). Blots were then developed using chemiluminescence (EZ-ECL, Biological Industries).

Global Tumor Vessel Perfusion. Murine ultrasonographic imaging was applied to measure global tumor vessel perfusion by using a three-dimensional (3D) imaging motor and color Doppler mode as described previously with minor modifications (37, 61). Briefly, mice were anesthetized with 2% isoflurane (RWD Life Science) and placed supine on a warmed platform. EO771 or LAP0297 tumors were visualized by using a Vevo 2100 Imaging System with 550D scan probe (VisualSonics, Inc.) at 32 MHz. The 3D mode recorded the *x*-, *y*-, and *z*-directions' data at 0.1 mm step size. The percentage of global tumor blood vessel perfusion over 3D tumor volume was analyzed according to the manufacturer's instructions.

Immunohistochemistry and Image Analysis. Tumor blood vessel staining and analysis was conducted as previously described with minor modifications (12, 37). Briefly, mice were intravenously injected with 200 μg Hoechst 33342 (Ho33342, Solarbio) per mouse. After circulation for 5 min, mice were intracardiacally perfused by Dulbecco's phosphate-buffered saline (PBS, Gibco). Tumor tissues were harvested and fixed by 4% paraformaldehyde (PFA) at room temperature for 2 to 3 h followed by incubation overnight with 30% sucrose at 4 °C. The tissues were then embedded in Tissue-Tek optimal cutting temperature compound and stored at −80 °C. The tumor tissue slices (20 μm thickness) were incubated overnight with primary antibodies at 4 °C followed by incubation with the secondary antibodies for 2 h at room temperature. All incubation processes were kept in dark and humid chambers. Primary antibodies included anti-CD31 (an endothelial cell marker, 1:100, clone MEC13.3, catalog 550274, BD Biosciences), anti-NG2 (a pericyte marker, 1:500, polyclonal, catalog AB5320, Sigma-Aldrich), anti-activated Notch1 (1:300, polyclonal, catalog ab8925, Abcam), anti-CD4 (1:50, clone GK1.5, catalog 100402, BioLegend), anti-CD8a (1:50, clone 53–6.7, catalog 100702, BioLegend), and anti-F4/80 (1:100, clone BM8, catalog 123101, BioLegend). Secondary antibodies included Alexa Fluor 488 Goat Anti-Armenian Hamster (catalog 127–545-160), Cy3 Goat Anti-Armenian Hamster (catalog 127–165-160), Alexa Fluor 647 Goat Anti-Armenian Hamster (catalog 127–605-160), Cy3-Donkey anti-Rabbit (catalog 711–165-152), Cy3-Donkey anti-Rat (catalog 712–165-153), and Cy5-Donkey anti-Rat (catalog 715–175-153) (1:200, all from Jackson ImmunoResearch). For hypoxia staining, tumor-bearing mice were injected intravenously with pimonidazole (60 mg/kg, 100 μL saline/mouse, Hypoxyprobe). After 25 min, mice were systemically perfused with 4% PFA, and the tumors were removed and immediately frozen in liquid nitrogen. Tumor sections were stained with a Hypoxyprobe Plus Kit according to the manufacturer's protocol (catalog HP8-100Kit). The slices were counter stained for cell nuclei by Sytox Green (catalog S7020, Molecular Probes). Sections were imaged with an Olympus FV3000 confocal laser-scanning microscope. The microvessel density, pericyte coverage, tissue hypoxia, and tissue area stained with Ho33342 were assessed using Image-Pro plus software (version 6.0).

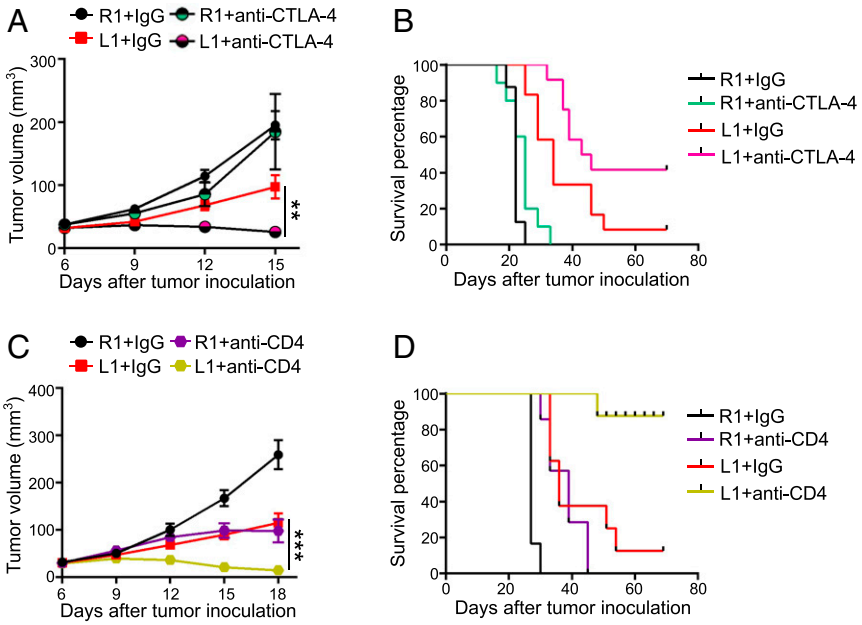

Fig. 7. Elevated levels of DLL1 in the TME improves anti-CTLA4 therapy. EO771-R1 and EO771-L1 breast tumors were prepared as described in Fig. 1. (*A* and *B*) The tumor growth curves and the survival of EO771-R1 and EO771-L1 tumor-bearing mice without or with anti-CTLA4 therapy. When tumors reached 4 to 5 mm in diameter, mice were randomly assigned to two groups and treated with an anti-CTLA4 antibody or control IgG (5 mg/kg) every 3 d for four doses. (*C* and *D*) The tumor growth curves and the survival of EO771-R1 and EO771-L1 tumor-bearing mice without or with $CD4^+$ T cell depletion. When tumors reached 3 to 4 mm in diameter, mice were randomly assigned to two groups and treated with an anti-CD4 antibody or control IgG (200 μg/mouse) on days 6, 8, and 14 post–tumor cell inoculation. The significance was determined by one-way ANOVA. Data are from one experiment representative of two independent experiments with similar results ($n = 10$ mice per group). $^{**}P < 0.01$, $^{***}P < 0.001$.

Flow Cytometric Analysis. Tumor-bearing mice were perfused via intracardiac injection of PBS after euthanasia. Tumor tissues were harvested and digested with DMEM containing collagenase type 1A (1.5 mg/mL, Sigma-Aldrich), hyaluronidase (1.5 mg/mL, Sigma-Aldrich), and deoxyribonuclease I (20 U/mL, Sigma-Aldrich) at 37 °C for 45 min. The digested mixtures were grinded and filtered through 70 μm cell strainers. After blocking with a rat anti-mouse CD16/CD32 antibody (BD Pharmingen), the single-cell suspensions were then stained, washed, and resuspended in cold flow buffer (1% bovine serum albumin and 0.1% NaN_3 in PBS). The following fluorochrome-conjugated antibodies were used: CD45-PE-Cy7, CD45-BV421, CD11b-BV510, CD11b-APC-Cy7, CD8a-PE-Cy7, and IFNγ-PE-Cy7 (all from BD Pharmingen); CD8a-FITC, F4/80-FITC, CD4-PE, PD-L1-PE, CD279-APC-Cy7, CD44-APC, CD62L-APC-Cy7, F4/80-PE, CD206-PE-Cy7, CD11c-APC, and Gr-1-APC-Cy7 (all from BioLegend). 7-Amino-actinomycin D (7AAD) (eBioscience) was used as viability dye to exclude death cells. For IFN-γ intracellular staining in CD4 or CD8 T cells, 1×10^6 cells were resuspended in 200 μL Roswell Park Memorial Institute 1640 medium containing 10% fetal bovine serum, 1% Penicillin-Streptomycin, and 1× Brefeldin A Solution (catalog 420601, eBioscience) and were incubated at 37 °C with 5% CO_2 for 4 h. Cells were collected for extracellular staining and then IFN-γ intracellular staining using a Fixation/Permeabilization Solution Kit (catalog 554714, BD Bioscience) per the manufacturer's instructions. Flow cytometry data were acquired on a Gallios flow cytometer (Beckman) and analyzed with Kaluza software (version 1.3).

Quantitative Real-Time PCR. Total messenger RNA was extracted from flow-sorted cells or tumor tissues using a MicroElute Total RNA kit (Omega). Complementary DNA (cDNA) was prepared by using a RevertAid First Strand cDNA Synthesis Kit (Thermo Scientific). Quantitative real-time PCR was performed using the Light Cycler 480 SYBR Green I Master mix (Roche) and a High Throughput qPCR Light Cycler 480 (Roche). Primers were provided in *SI Appendix*, Table S1. To avoid potential nonspecific amplification, one half of a primer sequence was designed to hybridize with the 3′ end of one exon, and the other half was hybridized to the 5′ end of the adjacent exon. The comparative threshold cycle method was used to calculate the fold changes of gene expression by normalizing to the reference gene β-actin.

Statistical Analysis. Statistical analyses were conducted by using Prism software (version 8, GraphPad). Experimental differences were tested using unpaired two-tailed Student's *t* test when comparing two independent groups and one-way ANOVA when comparing more than two groups. All of the data were presented as the mean ± SEM. The results were considered statistically significant when $P < 0.05$.

Data Availability. All study data are included in the article and *SI Appendix*.

ACKNOWLEDGMENTS. We are grateful to Dr. Jinping Zhang (Soochow University) for technical support. This work was supported in part by the National Program on Key Research Project of China 2016YFC1302400 (to Y.H.), the National Natural Science Foundation of China Grants 81972877 and 81372245 (to Y.H.), the State Key Laboratory of Radiation Medicine and Prevention (GZN1201904, to Y.H.), the Collaborative Innovation Center of Hematology, and the Priority Academic Program Development of Jiangsu Higher Education Institutions.

1. R. Ganss, B. Arnold, G. J. Hämmerling, Mini-review: Overcoming tumor-intrinsic resistance to immune effector function. *Eur. J. Immunol.* **34**, 2635–2641 (2004).
2. M. V. Sitkovsky, T regulatory cells: Hypoxia-adenosinergic suppression and re-direction of the immune response. *Trends Immunol.* **30**, 102–108 (2009).
3. G. T. Motz, G. Coukos, The parallel lives of angiogenesis and immunosuppression: Cancer and other tales. *Nat. Rev. Immunol.* **11**, 702–711 (2011).
4. R. K. Jain, Normalizing tumor microenvironment to treat cancer: Bench to bedside to biomarkers. *J. Clin. Oncol.* **31**, 2205–2218 (2013).
5. L. L. Munn, R. K. Jain, Vascular regulation of antitumor immunity. *Science* **365**, 544–545 (2019).
6. S. M. Hatfield, M. V. Sitkovsky, Antihypoxic oxygenation agents with respiratory hyperoxia to improve cancer immunotherapy. *J. Clin. Invest.* **130**, 5629–5637 (2020).
7. Y. Huang, S. Goel, D. G. Duda, D. Fukumura, R. K. Jain, Vascular normalization as an emerging strategy to enhance cancer immunotherapy. *Cancer Res.* **73**, 2943–2948 (2013).
8. S. M. Hatfield *et al.*, Immunological mechanisms of the antitumor effects of supplemental oxygenation. *Sci. Transl. Med.* **7**, 277ra30 (2015).
9. Y. Huang *et al.*, Improving immune-vascular crosstalk for cancer immunotherapy. *Nat. Rev. Immunol.* **18**, 195–203 (2018).
10. F. Winkler *et al.*, Kinetics of vascular normalization by VEGFR2 blockade governs brain tumor response to radiation: Role of oxygenation, angiopoietin-1, and matrix metalloproteinases. *Cancer Cell* **6**, 553–563 (2004).
11. J. Hamzah *et al.*, Vascular normalization in Rgs5-deficient tumours promotes immune destruction. *Nature* **453**, 410–414 (2008).

12. Y. Huang *et al*., Vascular normalizing doses of antiangiogenic treatment reprogram the immunosuppressive tumor microenvironment and enhance immunotherapy. *Proc. Natl. Acad. Sci. U.S.A.* **109**, 17561–17566 (2012).
13. N. Chauvet *et al*., Complementary actions of dopamine D2 receptor agonist and anti-vegf therapy on tumoral vessel normalization in a transgenic mouse model. *Int. J. Cancer* **140**, 2150–2161 (2017).
14. R. Fu *et al*., Inactivation of endothelial ZEB1 impedes tumor progression and sensitizes tumors to conventional therapies. *J. Clin. Invest.* **130**, 1252–1270 (2020).
15. S. La Porta *et al*., Endothelial Tie1-mediated angiogenesis and vascular abnormalization promote tumor progression and metastasis. *J. Clin. Invest.* **128**, 834–845 (2018).
16. A. G. Sorensen *et al*., Increased survival of glioblastoma patients who respond to antiangiogenic therapy with elevated blood perfusion. *Cancer Res.* **72**, 402–407 (2012).
17. X. Zheng *et al*., CTLA4 blockade promotes vessel normalization in breast tumors via the accumulation of eosinophils. *Int. J. Cancer* **146**, 1730–1740 (2020).
18. A. Johansson-Percival, B. He, R. Ganss, Immunomodulation of tumor vessels: It takes two to tango. *Trends Immunol.* **39**, 801–814 (2018).
19. P. Carmeliet, R. K. Jain, Molecular mechanisms and clinical applications of angiogenesis. *Nature* **473**, 298–307 (2011).
20. A. Sandler *et al*., Paclitaxel-carboplatin alone or with bevacizumab for non-small-cell lung cancer. *N. Engl. J. Med.* **355**, 2542–2550 (2006).
21. M. A. Socinski *et al*.; IMpower150 Study Group, Atezolizumab for first-line treatment of metastatic nonsquamous NSCLC. *N. Engl. J. Med.* **378**, 2288–2301 (2018).
22. F. Radtke, H. R. MacDonald, F. Tacchini-Cottier, Regulation of innate and adaptive immunity by Notch. *Nat. Rev. Immunol.* **13**, 427–437 (2013).
23. J. J. Hofmann, M. L. Iruela-Arispe, Notch signaling in blood vessels: Who is talking to whom about what? *Circ. Res.* **100**, 1556–1568 (2007).
24. E. Bridges, C. E. Oon, A. Harris, Notch regulation of tumor angiogenesis. *Future Oncol.* **7**, 569–588 (2011).
25. G. Thurston, I. Noguera-Troise, G. D. Yancopoulos, The delta paradox: DLL4 blockade leads to more tumour vessels but less tumour growth. *Nat. Rev. Cancer* **7**, 327–331 (2007).
26. M. Yan, Therapeutic promise and challenges of targeting DLL4/NOTCH1. *Vasc. Cell* **3**, 17 (2011).
27. F. Kuhnert, J. R. Kirshner, G. Thurston, Dll4-Notch signaling as a therapeutic target in tumor angiogenesis. *Vasc. Cell* **3**, 20 (2011).
28. C. Mailhos *et al*., Delta4, an endothelial specific notch ligand expressed at sites of physiological and tumor angiogenesis. *Differentiation* **69**, 135–144 (2001).
29. M. Yan, G. D. Plowman, Delta-like 4/Notch signaling and its therapeutic implications. *Clin. Cancer Res.* **13**, 7243–7246 (2007).
30. N. S. Patel *et al*., Up-regulation of endothelial delta-like 4 expression correlates with vessel maturation in bladder cancer. *Clin. Cancer Res.* **12**, 4836–4844 (2006).
31. M. Yan *et al*., Chronic DLL4 blockade induces vascular neoplasms. *Nature* **463**, E6–E7 (2010).
32. X. Q. Yan *et al*., A novel Notch ligand, Dll4, induces T-cell leukemia/lymphoma when overexpressed in mice by retroviral-mediated gene transfer. *Blood* **98**, 3793–3799 (2001).
33. I. Maillard, S. H. Adler, W. S. Pear, Notch and the immune system. *Immunity* **19**, 781–791 (2003).
34. Y. Huang *et al*., Resuscitating cancer immunosurveillance: Selective stimulation of DLL1-notch signaling in T cells rescues T-cell function and inhibits tumor growth. *Cancer Res.* **71**, 6122–6131 (2011).
35. B. Z. Qian, J. W. Pollard, Macrophage diversity enhances tumor progression and metastasis. *Cell* **141**, 39–51 (2010).
36. M. Locati, G. Curtale, A. Mantovani, Diversity, mechanisms, and significance of macrophage plasticity. *Annu. Rev. Pathol.* **15**, 123–147 (2020).
37. X. Zheng *et al*., Increased vessel perfusion predicts the efficacy of immune checkpoint blockade. *J. Clin. Invest.* **128**, 2104–2115 (2018).
38. L. Tian *et al*., Mutual regulation of tumour vessel normalization and immunostimulatory reprogramming. *Nature* **544**, 250–254 (2017).
39. M. Nishino, N. H. Ramaiya, H. Hatabu, F. S. Hodi, Monitoring immune-checkpoint blockade: Response evaluation and biomarker development. *Nat. Rev. Clin. Oncol.* **14**, 655–668 (2017).
40. S. L. Topalian, J. M. Taube, R. A. Anders, D. M. Pardoll, Mechanism-driven biomarkers to guide immune checkpoint blockade in cancer therapy. *Nat. Rev. Cancer* **16**, 275–287 (2016).
41. T. R. Simpson *et al*., Fc-dependent depletion of tumor-infiltrating regulatory T cells co-defines the efficacy of anti-CTLA-4 therapy against melanoma. *J. Exp. Med.* **210**, 1695–1710 (2013).
42. E. Romano *et al*., Ipilimumab-dependent cell-mediated cytotoxicity of regulatory T cells ex vivo by nonclassical monocytes in melanoma patients. *Proc. Natl. Acad. Sci. U.S.A.* **112**, 6140–6145 (2015).
43. R. S. Finn *et al*.; IMbrave150 Investigators, Atezolizumab plus bevacizumab in unresectable hepatocellular carcinoma. *N. Engl. J. Med.* **382**, 1894–1905 (2020).
44. W. Jiang, Y. Huang, Y. An, B. Y. Kim, Remodeling tumor vasculature to enhance delivery of intermediate-sized nanoparticles. *ACS Nano* **9**, 8689–8696 (2015).
45. Y. Huang, T. Stylianopoulos, D. G. Duda, D. Fukumura, R. K. Jain, Benefits of vascular normalization are dose and time dependent—letter. *Cancer Res.* **73**, 7144–7146 (2013).
46. R. K. Jain, Antiangiogenesis strategies revisited: From starving tumors to alleviating hypoxia. *Cancer Cell* **26**, 605–622 (2014).
47. T. Kammertoens *et al*., Tumour ischaemia by interferon-γ resembles physiological blood vessel regression. *Nature* **545**, 98–102 (2017).
48. C. C. Caldwell *et al*., Differential effects of physiologically relevant hypoxic conditions on T lymphocyte development and effector functions. *J. Immunol.* **167**, 6140–6149 (2001).
49. D. W. Hoskin, T. Reynolds, J. Blay, Adenosine as a possible inhibitor of killer T-cell activation in the microenvironment of solid tumours. *Int. J. Cancer* **59**, 854–855 (1994).
50. A. Ohta, M. Sitkovsky, Role of G-protein-coupled adenosine receptors in downregulation of inflammation and protection from tissue damage. *Nature* **414**, 916–920 (2001).
51. S. M. Hatfield *et al*., Systemic oxygenation weakens the hypoxia and hypoxia inducible factor 1α-dependent and extracellular adenosine-mediated tumor protection. *J. Mol. Med. (Berl.)* **92**, 1283–1292 (2014).
52. F. Mpekris *et al*., Combining microenvironment normalization strategies to improve cancer immunotherapy. *Proc. Natl. Acad. Sci. U.S.A.* **117**, 3728–3737 (2020).
53. S. Welsh, R. Williams, L. Kirkpatrick, G. Paine-Murrieta, G. Powis, Antitumor activity and pharmacodynamic properties of PX-478, an inhibitor of hypoxia-inducible factor-1alpha. *Mol. Cancer Ther.* **3**, 233–244 (2004).
54. A. L. Doedens *et al*., Hypoxia-inducible factors enhance the effector responses of CD8(+) T cells to persistent antigen. *Nat. Immunol.* **14**, 1173–1182 (2013).
55. A. Palazon *et al*., An HIF-1α/VEGF-A Axis in cytotoxic T cells regulates tumor progression. *Cancer Cell* **32**, 669–683.e5 (2017).
56. T. Cramer *et al*., HIF-1alpha is essential for myeloid cell-mediated inflammation. *Cell* **112**, 645–657 (2003).
57. J. P. Zhang *et al*., Overexpression of Notch ligand Dll1 in B16 melanoma cells leads to reduced tumor growth due to attenuated vascularization. *Cancer Lett.* **309**, 220–227 (2011).
58. X. C. Zhao *et al*., Inhibition of tumor angiogenesis and tumor growth by the DSL domain of human Delta-like 1 targeted to vascular endothelial cells. *Neoplasia* **15**, 815–825 (2013).
59. E. E. Tchekneva *et al*., Determinant roles of dendritic cell-expressed Notch Delta-like and Jagged ligands on anti-tumor T cell immunity. *J. Immunother. Cancer* **7**, 95 (2019).
60. P. Huang, D. G. Duda, R. K. Jain, D. Fukumura, Histopathologic findings and establishment of novel tumor lines from spontaneous tumors in FVB/N mice. *Comp. Med.* **58**, 253–263 (2008).
61. A. Pistner, S. Belmonte, T. Coulthard, B. Blaxall, Murine echocardiography and ultrasound imaging. *J. Vis. Exp.* **42**, e2100 (2010).